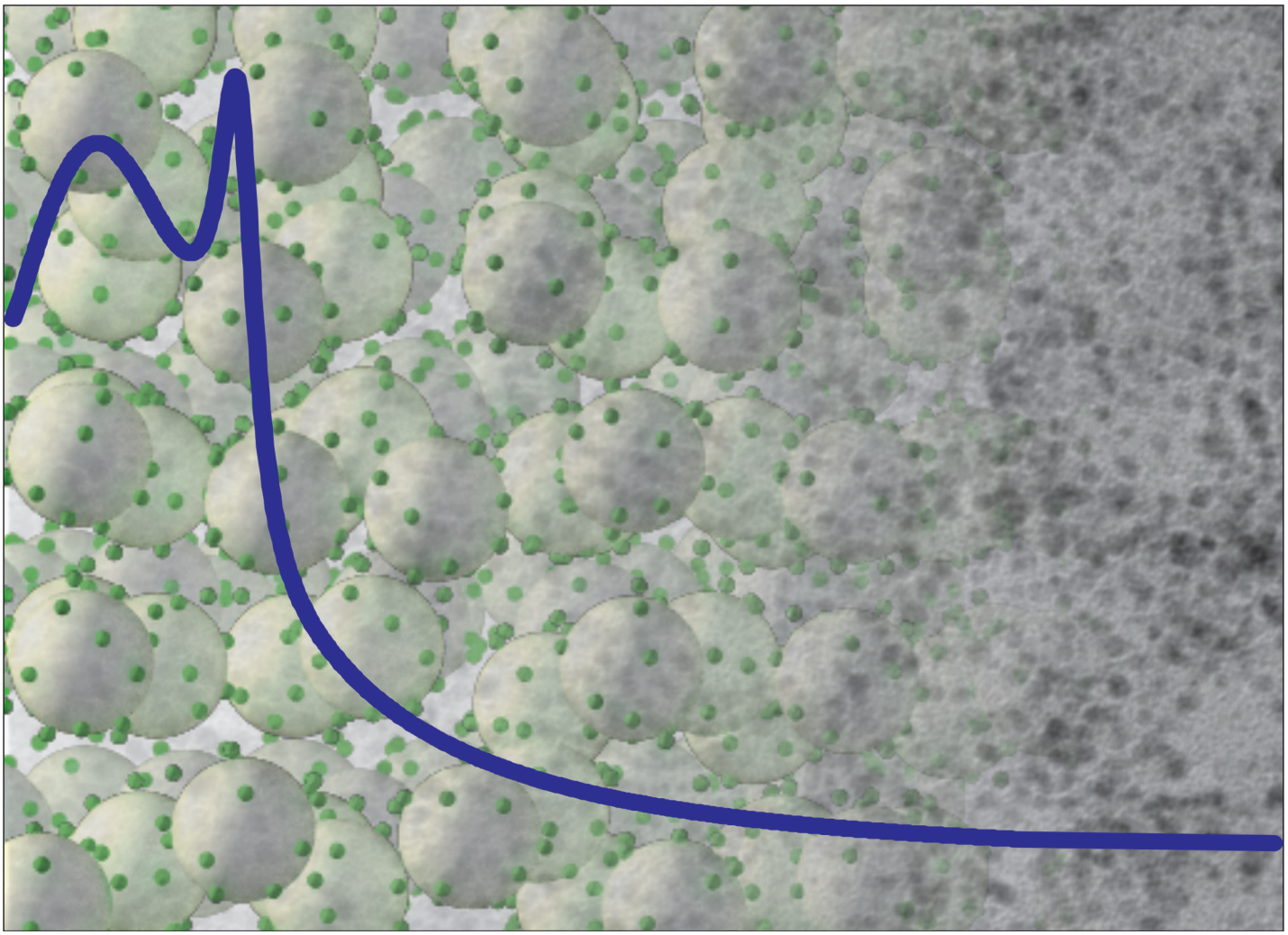

**Showcasing research from the Multifunctional Optical Materials group at the Institute of Materials Science of Seville, Spain.**

Determination of the optical constants of ligand-free organic lead halide perovskite quantum dots

Herein we demonstrate a method to determine the complex refractive index of $MAPbBr_3$ and $MAPbI_3$ perovskite quantum dots (QDs). We take advantage of a scaffold-based, ligand-free, synthetic approach that gives rise to transparent composite films that allow a clean analysis of the QD optical constants, without the interference of organic layers. These results may be used to achieve a finer design and optimization of perovskite quantum dot optoelectronic devices.

## As featured in:

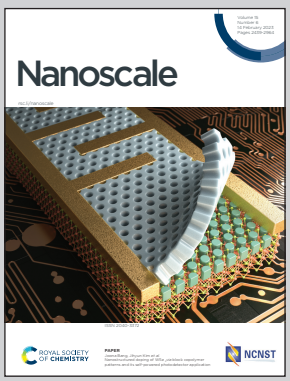


See Hernán Míguez *et al.*, *Nanoscale*, 2023, **15**, 2553.

ROYAL SOCIETY OF CHEMISTRY

rsc.li/nanoscale

Registered charity number: 207890

Nanoscale

COMMUNICATION

View Article Online
View Journal | View Issue



Cite this: *Nanoscale*, 2023, **15**, 2553

Received 16th September 2022,
Accepted 1st November 2022

DOI: 10.1039/d2nr05109e

rsc.li/nanoscale

# Determination of the optical constants of ligand-free organic lead halide perovskite quantum dots†

Andrea Rubino, Gabriel Lozano, Mauricio E. Calvo and Hernán Míguez *

**Precise knowledge of the optical constants of perovskite lead halide quantum dots (QDs) is required to both understand their interaction with light and to rationally design and optimize the devices based on them. However, their determination from colloidal nanocrystal suspensions, or films made out of them, remains elusive, as a result of the difficulty in disentangling the optical constants of the organic capping ligands and those of the semiconductor itself. In this work, we extract the refractive index and extinction coefficient of ligand-free methylammonium lead iodide ($MAPbI_3$) and bromide ($MAPbBr_3$) nanocrystals. In order to prevent the use of organic ligands in the preparation, we follow a scaffold assisted synthetic procedure, which yields a composite film of high optical quality that can be independently and precisely characterized and modelled. In this way, the contribution of the guest nanocrystals can be successfully discriminated from that of the host matrix. Using a Kramers–Kronig consistent dispersion model along with an effective medium approximation, it is possible to derive the optical constants of the QDs by fitting the spectral dependence of light transmitted and reflected at different angles and polarizations. Our results indicate a strong dependence of the optical constants on the QD size. Small nanocrystals show remarkably large values of the extinction coefficient compared to their bulk counterparts. This analysis opens the door to the rigorous modelling of solar cells and light-emitting diodes with active layers based on perovskite QDs.**

## Introduction

The determination of the optical constants (*i.e.*, refractive index and extinction coefficient) of semiconductors is essential to model their interaction with light, which is also central to the optimization of the performance of optoelectronic devices. They are typically determined from the analysis of the optical response of the materials with the aid of appropriate models.[1–8] As far as lead halide perovskites are concerned, several studies have focused on the characterization of their optical constants.[8–17] Remarkably, a comparative analysis reveals that significant dispersion is observed for materials that are nominally the same, which is mainly attributed to differences in sample preparation.[18] As far as we know, to date, all reported works have focused on the analysis of the optical constants of perovskites in the shape of thin films or single crystals. However, the determination of the complex refractive index of perovskite nanocrystals remains elusive. This contrasts with their relevance in different applied research fields, such as light-emitting diodes,[19,20] solar cells,[21,22] transistors,[23] photodetectors[24] and, more recently, X-ray detection,[25] or non-linear optics,[26,27] which could greatly benefit from optimized designs that require a precise knowledge of the optical constants of all materials involved, as it has been demonstrated for their bulk counterparts.[15,16,28]

In order to perform a reliable determination of the optical constants of a material, uniform and scattering-free films are required. However, the preparation of such films out of colloidal nanocrystals, which are typically attained by ligand-assisted synthesis,[29,30] is not straightforward. Furthermore, the structural configuration of the ligand network in a film made of colloidal nanocrystals is strongly dependent on the interaction between them, which depends in turn on the processing of the sample. So, even if high quality films can be obtained, since both sets of optical constants (*i.e.*, that of the nanocrystals and the one corresponding to the ligand network) are unknown, discriminating between their relative contributions to the overall optical response of a quantum dot solid is not an easy task.[31–34] On the other hand, it has been recently demonstrated that optoelectronic quality perovskite QDs can be achieved within the void network of pore size controlled metal oxide matrices.[35] Moreover, these can be made in

*Instituto de Ciencia de Materiales de Sevilla (CSIC-US), C/Américo Vespucio 49, 41092 Sevilla, Spain. E-mail: h.miguez@csic.es*

†Electronic supplementary information (ESI) available: Details of the Tauc plot analysis; the use of the Brus equation; the experimental quantification of the QD filling fraction; the modeling of the complex refractive index; the extracted dielectric constants; the comparison between different effective medium approximations. See DOI: https://doi.org/10.1039/d2nr05109e

the shape of homogeneous and uniform scattering-free films,[36,37] which opens the possibility to perform specular reflection and ballistic transmission measurements that allow a precise estimation of their average optical constants as reliable as those attained by ellipsometry characterization.[38,39] Since in this case both the optical constants and the volume fraction of the host are known, it may be possible to differentiate the contribution from the semiconductor nanocrystals and determine their optical constants in a reliable way.

Based on this hypothesis, in this work we obtain the optical constants of ligand-free $MAPbI_3$ and $MAPbBr_3$ QDs embedded in porous scaffolds. The transparent porous films employed as hosts provide the necessary environmental stability required to perform reliable characterization of their optical properties without the need for ligands. A combination of a Forouhi–Bloomer model, employed to describe the spectral dependence of the complex refractive index of the QDs, and an effective medium approximation, accounting for the interaction between perovskite NCs and the porous silica matrix, is employed to fit the optical reflectance and transmittance measured at different angles from a series of QD embedded films[40] and extract their optical constants. Interestingly, our analysis reveals that QD size reduction brings about an increase in the extinction coefficient. Our results not only provide information on the fundamental constants of nanosized organic lead halides, but also open the door to precise modelling of perovskite QD-based optoelectronic devices.

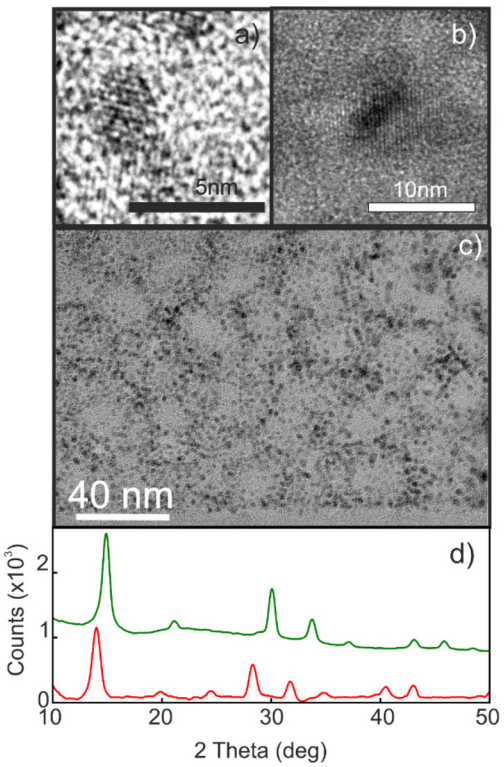


**Fig. 1** (a and b) High-resolution TEM micrographs of $MAPbBr_3$ (a) and $MAPbI_3$ (b) nanocrystals inside a porous silica matrix. (c) The TEM cross section of the QD-$MAPbBr_3$@$SiO_2$ composite layer. (d) XRD diffractograms of QD-$MAPbBr_3$@$SiO_2$ (green line) and QD-$MAPbI_3$@$SiO_2$ (red line). For the sake of clarity, backgrounds were subtracted in both diffractograms.

## Results and discussion

### Nanocrystal synthesis and characterization

Porous silicon oxide films exhibiting plane-parallel interfaces and a high transparency, with a thickness $d$ of ~400 nm, were used as scaffolds for the synthesis of $MAPbBr_3$ and $MAPbI_3$ QDs analyzed in this work, following a procedure thoroughly described before.[37] Fig. 1(a and b) show the transmission electron microscopy (TEM) images of these films. Fig. 1c shows a typical TEM cross section of a focused ion beam cleaved and thinned lamella of a quantum dot filled porous silica scaffold (QD-$MAPbBr_3$@$SiO_2$) film, in which the semiconductor nanocrystals can be identified as dark spots inside the matrix. X-ray diffractograms confirm the presence of perovskite crystallites, as illustrated in Fig. 1d, with the main peaks associated with bromide- and iodide-based perovskites being clearly observed around $2\theta = 14.9°$ and $2\theta = 14.1°$, respectively.[41] Fig. 2 shows the corresponding photoluminescence (PL) spectra recorded from QD-$MAPbBr_3$@$SiO_2$ (Fig. 2a) and QD-$MAPbI_3$@$SiO_2$ (Fig. 2b). The PL spectra of the thin films of the bulk perovskite materials are also shown in Fig. 2a and b, for the sake of comparison. The characteristic gradual blue-shift of the electronic band gap is observed as the size of either $MAPbI_3$ or $MAPbBr_3$ nanocrystals becomes smaller. The average QD diameters were estimated both from the analysis of HRTEM images and by fitting the spectral position of the luminescence peak to the Brus model,[42] which offer consistent results (full details of the fittings can be found in the ESI†). The absorbance of these films was also estimated by measuring the total reflectance ($R_T$) and transmittance ($T_T$), and according to the formula $A = 1 - R_T - T_T$. Fig. 2c and d show the Tauc plots obtained for the different samples, which allow us to estimate the band gap energy ($E_g$) plotted *versus* the QD diameters in Fig. 2e and f.[43,44] A maximum blue-shift of ~100 meV is observed for the smallest QDs synthesized with respect to the $E_g$ of the bulk materials in each case.

### Determination of the optical constants

In order to extract the optical constants of the QDs, we measured the spectral dependence of light reflected and transmitted at different angles for both polarizations of the incident beam and fitted it using a model based on the transfer matrix formalism.[15] This method, which has been successfully employed in recent years to calculate the optical constants of homogeneous $ABX_3$ perovskite films or single crystals, constitutes a robust alternative to ellipsometry,[15,39] and has been applied to optimize the photo-conversion performance of high-efficient perovskite solar cells prepared by solution processing or evaporation.[16,28] In the present work, our model considers a system composed of a thin film (the porous silica matrix loaded with QDs) characterized by a thickness $d$ and a

 

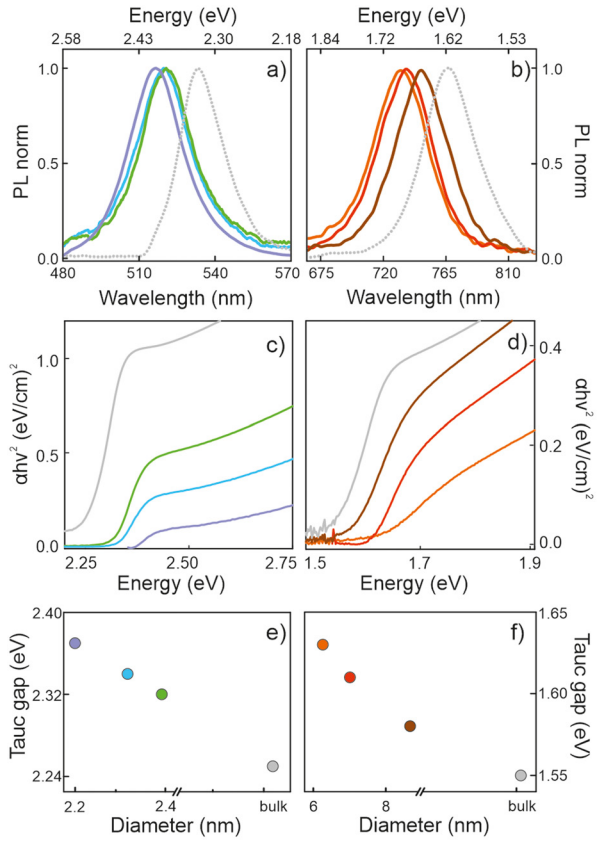


**Fig. 2** (a and b) The normalized PL spectra of $MAPbBr_3$ (a) and $MAPbI_3$ (b) QDs dispersed inside the porous films. All emissions were blue-shifted with respect to the spectral position of the bulk emission (grey dashed lines). (c) The Tauc plots of the $MAPbBr_3$@$SiO_2$ films, where the nanocrystal sizes are 2.4 nm (green line), 2.3 nm (blue line) and 2.2 nm (violet line). (d) The Tauc plots of the $MAPbI_3$@$SiO_2$ films, where the nanocrystal sizes are 9 nm (brown line), 7 nm (red line) and 6 nm (orange line). Grey lines represent the Tauc plots of the respective bulk films. (d and e) Size dependence of the Tauc gap ($E_g$ extracted from the Tauc plots) for the $MAPbBr_3$ (e) and $MAPbBr_3$ (f) QDs (color code as in (c) and (d)).

complex effective refractive index, $N_{eff} = n + ik$. A substrate of a refractive index 1.51 and thickness 1 mm is also assumed, while air is taken as the incoming and outgoing medium. In order to calculate the real ($n$) and imaginary ($k$) parts of $N_{eff}$, we use the approach developed by Maxwell and Garnett (MG), a well-established effective medium approximation that has been successfully employed recently to attain the $N_{eff}$ of colloidal quantum dot solid films.[31] In our case, both pores and perovskite nanocrystals are considered inclusions in the silica matrix.[45] For the calculations, we first experimentally determined the volume filling fractions of both the porous scaffold ($ff_{SiO_2}$) and the perovskite QDs ($ff_{QD}$). As the porous matrix can be analyzed independently[46] before infiltrating the QDs, $ff_{SiO_2}$ could be set at 0.51 and the (almost dispersion-less) refractive index of the solid part of the porous network at $N_{SiO_2} = 1.49$, as extracted by using a Cauchy model. Also, $ff_{QD}$ could be experimentally determined by means of inductively coupled plasma optical emission spectrometry (ICP-OES) for each film, as shown in Table S1 of the ESI,† where full details on this procedure can be found. Please note that the possibility to know the exact volume fraction and optical constants of the matrix, as well as the amount of nanocrystals present, implies a fundamental difference with respect to the optical analysis of the colloidal quantum dot solids. In the latter, the degree of interpenetration of the ligands surrounding the QDs is unknown, which prevents an accurate estimation of both the filling fraction and the optical constants of such organic networks, thus rendering the elucidation of the contribution of each one of the constituents to $N_{eff}$ unfeasible.

Considering this information, a Kramers–Kronig consistent Forouhi–Bloomer dispersion model, in the Jobin Yvon parametrization (new amorphous),[47] was used to account for the spectral dependence of the complex refractive index of the QDs. To find the set of parameters that fit best the optical response of the fabricated films, we combined our optical model with a genetic algorithm. Fig. 3 shows the calculated specular reflectance ($R$), ballistic transmittance ($T$) and absorbance ($A = 1 - R - T$) spectra for the best fitting obtained for a bulk film and for a porous silica layer scaffold loaded with 2.2 nm $MAPbBr_3$ (Fig. 3a and c) and 6 nm $MAPbI_3$ (Fig. 3b and d) nanocrystals, along with their corresponding experimental spectra (the results for QDs of different sizes are provided in the ESI†). A fair agreement is found and the main spectral features are faithfully reproduced. The slight divergence observed in the reflectance background can be attributed to a small fraction of diffusely scattered light due to the roughness or imperfections

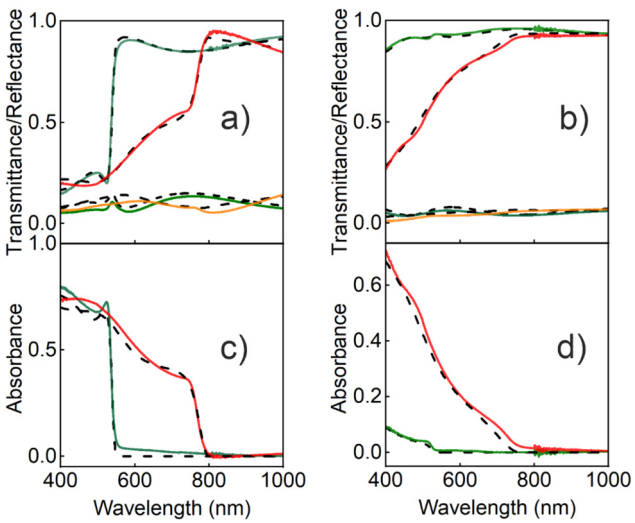


**Fig. 3** (a) The transmittance and reflectance spectra recorded for $MAPbBr_3$ (light and dark green lines, respectively) and $MAPbI_3$ (red and orange lines, respectively) bulk films, and (b) the transmittance and reflectance spectra recorded for nc-$MAPbBr_3$@$SiO_2$ (light and dark green lines, respectively) and nc-$MAPbI_3$@$SiO_2$ films (red and orange lines, respectively). The absorbance spectra obtained from the $R$ and $T$ measurements ($A = 1 - R - T$) for (c) the $MAPbBr_3$ and $MAPbI_3$ bulk films (dark green and red lines, respectively) and (d) the $MAPbBr_3$ and $MAPbI_3$ nanocrystal films (dark green and red lines, respectively). In all graphs, dashed black lines indicate the corresponding theoretical fittings.

in the film. The full set of parameters used for the calculation can also be found in the ESI.†

Fig. 4 shows the spectral dependence of both $n$ and $k$ of the $MAPbBr_3$ and $MAPbI_3$ QDs that provide the best fit to the experimental results. For comparison, we also show the data obtained for the corresponding bulk films, which are in accordance with the optical constants previously reported for such materials.[8,10] Complementarily, the spectral dependence of the real and imaginary parts of the corresponding complex dielectric constants are shown in the ESI.† Interestingly, a remarkable increase of both the real and imaginary parts of the refractive index occurs for energies above the band gap as the nanocrystal dimensions diminish. It is worth noting that this observation is independent of the approach employed to extract the optical constants. We employed a MG approach because it is the one that assumes a low filling fraction of the inclusions, as it is the case for the scaffold supported perovskite QDs used here (see Table S1†), and hence is expected to describe our system best. In fact, among all the possible ones tested, this approach provides the best fitting to our experimental results, thus supporting the validity of this assumption. In any case, for the sake of comparison, we have modelled the effective refractive index of the porous silica film loaded with QDs using other approximations. Regardless of the quantitative differences observed, the trends observed, and hence our main conclusions, are independent of the approximation chosen to model the effective index of the QD loaded scaffolds. More details may be found in the ESI (Fig. S2),† where comparisons to the results attained employing other approaches (more specifically, Bruggeman's model and a variant of MG assuming a homogeneous matrix as the host, instead of considering the pores as inclusions) are shown.

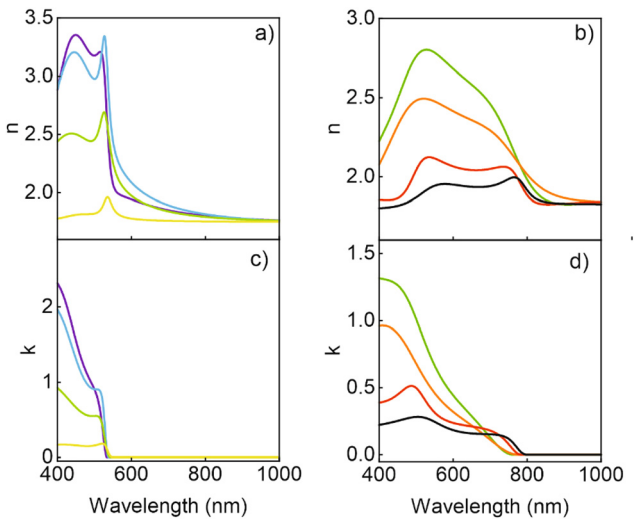


Fig. 4 The refractive index (a and b) and extinction coefficient (c and d) calculated for the ligand-free quantum dots of different composition and size. (a and c) $MAPbBr_3$ QDs (green line, QD size: 2.4 nm; blue line, 2.3 nm; violet line, 2.2 nm) and a polycrystalline film (yellow line). (b and d) $MAPbI_3$ QDs (red line, 9 nm; orange line, 7 nm; green line, 6 nm) and a polycrystalline film (black line).

## Analysis of the results

We observed an increase in the extinction coefficient of the first excitonic transition when the size of the QD decreased, an effect that is attributed to the higher oscillator strength, $f_1$, that results from the stronger overlap of the confined electron and hole and that has been thoroughly scrutinized before for other nanocrystalline semiconductors.[48] Under strong coupling, it has been shown that the oscillator strengths of the first exciton of a nanocrystal, $f_{nc1}$, and the bulk material, $f_{b1}$, are related by the expression:[49]

$$f_{nc1} \approx C\left(\frac{a_B}{r}\right)^3 f_{b1}, \quad (1)$$

where $a_B$ and $r$ stand for the exciton Bohr radius and the QD radius, respectively, and $C$ is a constant that depends on the geometry of the nanocrystals and the overlap of the electron and hole wavefunctions. The oscillator strength, in turn, can be estimated by:[50]

$$f = 4.318 \times 10^{-9} \cdot \int \varepsilon(q)\mathrm{d}q \quad (2)$$

where $\varepsilon(q)$ is the molar absorption coefficient expressed in the wavenumber scale, which we can estimate from the experimental determination of the absorbance (Abs), the film thickness, $l$, and the concentration of perovskite ($C_{ABX3}$) by ICP-OES in the different samples:

$$\varepsilon(q) = \frac{\mathrm{Abs}(q)}{l \cdot C_{ABX3}} (\mathrm{M}^{-1}\,\mathrm{cm}^{-2}). \quad (3)$$

The ratio $f_{nc1}/f_{b1}$ is evaluated employing the first oscillator that contributes to the fitting of $k$ and $n$ shown in Fig. 4 for both the nanocrystals and the bulk. From them, the corresponding Abs($q$), and then $\varepsilon(q)$ as given in eqn (3), are calculated. This information is used to attain $f_{nc1}$ for each QD size and $f_{b1}$ using eqn (2). The results of $f_{nc1}/f_{b1}$ *vs.* diameter for each perovskite QD sample under analysis can be seen in Fig. 5(a) and (b) (same color code as in Fig. 2), together with the expected inverse cubic dependence predicted using eqn (1). Assuming values of $a_B$ for $MAPbI_3$ (4.6 nm) and for $MAPbBr_3$ (3.8 nm), as reported in the literature,[51] the values of the constant $C$ attained from the fitting of the experimental data were 0.38 and 0.44, respectively, of the same order than the others reported in the literature. Please note that eqn (3) relies on the validity of the Lambert–Beer formula to account for the spatial decay of the transmitted light intensity along a homogeneous medium. However, in thin films with widths comparable to the light wavelength, the interference effects between counterpropagating light beams, which result from the partial transmission and reflection at each one of the film interfaces, may alter the commonly considered decaying exponential profile, hence limiting its applicability. In our case, this might give rise to certain deviations with respect to theoretical predictions.

Finally, for energies higher than the band gap, the extinction coefficient $k$ of solution dispersed quantum dots is

 

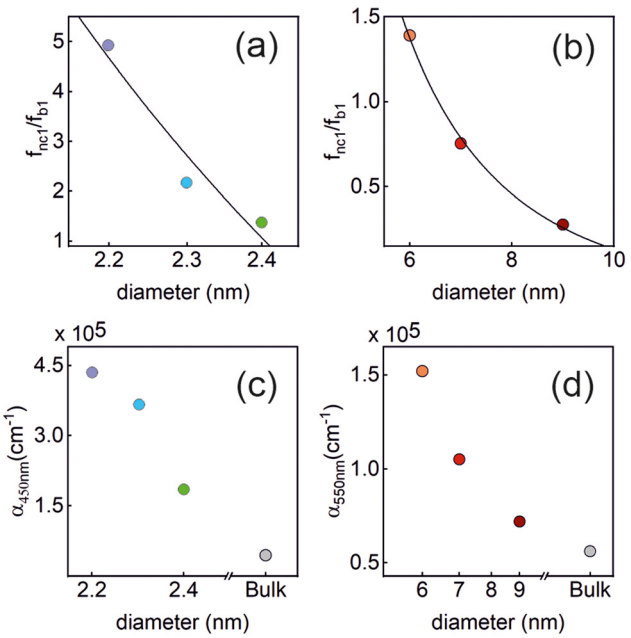


**Fig. 5** Upper panels: the normalized oscillator strength of the first excitonic transition *vs.* the QD size, estimated for the (a) $MAPbBr_3$ QDs, and (b) $MAPbI_3$ QDs using the values of $k$ extracted from our analysis. The solid line represents the theoretically expected $C\left(\frac{a_B}{r}\right)^3$ dependence. Lower panels: the absorption coefficient $\alpha$ *vs.* the QD size estimated for the (c) $MAPbBr_3$ QDs (at $\lambda$ = 450 nm), and (d) $MAPbI_3$ QDs (at $\lambda$ = 550 nm). In each plot, the color code is the same as that shown in Fig. 2.

expected to become size independent.[52,53] Our observations are at odds with this prediction, as shown in Fig. 5(c) and (d), in which we have plotted the absorption coefficient $\alpha$ for the $MAPbBr_3$ (at $\lambda$ = 450 nm) and $MAPbI_3$ (at $\lambda$ = 550 nm) QDs according to the following expression:

$$\alpha = \frac{4\pi k}{\lambda}. \quad (4)$$

One possible origin for this discrepancy may be that in our case the concentration is at orders of magnitude larger than those in the diluted dispersions (typically $10^{-6}$ M) commonly employed for this analysis, where QDs barely interact with each other. In our films, nanocrystals are close enough to allow a dot-to-dot charge transport.[35] Under these conditions, the neighbouring QDs are coupled through a dipolar interaction, which gives rise to an increase in the absorption cross section, and the polarization field induced by each nanoparticle may influence the surrounding nanoparticles. It has also been demonstrated that the dielectric confinement gives rise to an increase of the oscillator strength and therefore in the absorption cross section.[54] For instance, as a result of these interactions, it has been shown that QD solids made out of colloidal CdSe and PbS monolayers present an absorption increase as the size of the nanocrystals and ligands decreases.[32,55] Also, composite nanostructures that resemble those herein studied show an increase in the absorption of the QDs embedded in matrices with a lower dielectric constant, such as PbS in a glass matrix,[56] PbS/FAPI systems[57] and $CsPbBr_3$ NCs embedded in a $Cs_4PbBr_6$ matrix.[58]

## Conclusion

Herein, we demonstrate a method to determine the complex refractive indexes of $MAPbBr_3$ and $MAPbI_3$ perovskite quantum dots. To the best of our knowledge, the results attained constitute the first set of optical constants that can be considered intrinsic to these nanosized semiconductors. This achievement was possible due to the precise knowledge of the nanocrystal dielectric environment, which could be seized due to both the absence of capping ligands and the possibility to extract independently the optical constants of the host matrix in which the embedded nanocrystals are synthesized. We use a Kramers–Kronig consistent model to account for the spectral dispersion of the complex refractive index of the nanocrystals and an effective medium approximation approach to consider the effect of the porous silica matrix in which the nanocrystals are dispersed. Hence, contributions from the host and guest could be differentiated. Our analysis consistently reveals a remarkable increase of the values of both the real and the imaginary parts of the refractive index as the size of nanocrystals reduces. While the increase of the oscillator strength of the first excitonic transition grows according to the theoretical predictions; the behavior at energies well above the band gap edge is anomalous, but characteristic of QDs embedded in a vitreous host. We believe our results are both relevant from a fundamental perspective, as they provide a deeper insight into the origin of the remarkable optical properties of lead halide perovskites, and useful from an applied point of view, since they will allow a finer design and optimization of the optoelectronic devices in which perovskite QDs are already widely used.

## Methods

### Perovskite@$SiO_2$ composite preparation

The porous $SiO_2$-based thin film consists of a stratification of Ludox TMA nanoparticles (30 nm) deposited by dip-coating onto a microslide glass substrate up to a 400 nm thickness with a final calcination step (400 °C). The $MAPbX_3$ precursor solution contains a mixture of MAX and $PbBr_2$ or $PbCl_2$ (where X is Br or I), respectively, for bromide and iodide perovskites. Precursors were dissolved in *N*,*N*-dimethylformamide at a molar ratio of 3 to 1. Typically, for each case, the same recipes are employed for the preparation of the corresponding polycrystalline films, depositing the most concentrated precursor solution on the substrate, without the $SiO_2$ porous layer. NC synthesis is a one-pot process conducted in a glovebox, in which the precursor solution (different concentration for each NC) is dropped on top of the silica matrix and spin coated. Finally, the composite is heated up to 100 °C for 40 min.

### Structural characterization

Lead determination was carried out by atomic emission spectroscopy with an inductively coupled plasma (ICP OES JASCO FT/IR-6200 IRT-5000). The microscopic analysis illustrated in Fig. 1 was performed using a FEI Talos F200S scanning/transmission electron microscope to observe the sample lamellae prepared by means of a focused ion beam (FIB, Carl Zeiss Auriga). For the composite thickness measurements, we used a profilometer.

### Optical characterization

The photoluminescence spectra were recorded using a spectrophotometer, using two different lasers at 450 nm and 530 nm for the excitation of $MAPbBr_3$ and $MAPbI_3$, respectively. The $R_T$ and $T_T$ measurements were carried out inside an integrating sphere (DRA-2500, Agilent) connected to a commercial spectrophotometer (Cary 5000 UV-Vis-NIR). For the angular characterization, we made use of an accessory of the spectrophotometer, which is the Universal Measurement Accessory, allowing the analysis of the angular optical response of the composite films.

### Complex refractive index determination

We fitted the optical response of the layers using an optical model based on the transfer matrix formalism. To model the spectral dependence of the nanocrystals, we used the Forouhi–Bloomer model in the Jobin–Yvon parametrization. Specifically, we considered three oscillators for $MAPbI_3$ and two oscillators for $MAPbBr_3$. Besides, we used an effective medium approximation to model the effective refractive index of the porous silica layer in which nanocrystals were embedded. A genetic algorithm was used to look for the parameters that provide the best fit for the experimental data. The results are shown in the ESI.†

## Data availability

Data for this paper are available at Digital CSIC at **https://doi.org/10.20350/digitalCSIC/14799**. The code for estimating the optical constants of an arbitrary layered optical material may be found at **https://github.com/Multifunctional-Optical-Materials-Group**.

## Conflicts of interest

There are no conflicts to declare.

## Acknowledgements

Financial support from the Spanish Ministry of Science and Innovation under grant PID2020-116593RB-I00, funded by MCIN/AEI/10.13039/501100011033, and from the Junta de Andalucía under grant P18-RT-2291 (FEDER/UE) is gratefully acknowledged.

## References

1 J. I. Cisneros, Optical characterization of dielectric and semiconductor thin films by use of transmission data, *Appl. Opt.*, 1998, **37**, 5262–5270.
2 D. Poelman and D. F. Smet, Methods for the determination of the optical constants of thin films from single transmission measurements: a critical review, *J. Phys. D: Appl. Phys.*, 2003, **36**, 1850.
3 I. Moreels, K. Lambert, D. De Muynck, F. Vanhaecke, D. Poelman, J. C. Martins, G. Allan and Z. Hens, Composition and Size-Dependent Extinction Coefficient of Colloidal PbSe Quantum Dots, *Chem. Mater.*, 2007, **19**, 6101–6106.
4 I. Moreels, K. Lambert, D. Smeets, D. De Muynck, T. Nollet, J. C. Martins, F. Vanhaecke, A. Vantomme, C. Delerue, G. Allan and Z. Hens, Size-Dependent Optical Properties of Colloidal PbS Quantum Dots, *ACS Nano*, 2009, **3**, 3023–3030.
5 Z. Hens and I. Moreels, Light absorption by colloidal semiconductor quantum dots, *J. Mater. Chem.*, 2012, **22**, 10406–10415.
6 Y. C. Liu, J. H. Hsieh and S. K. Tung, Extraction of optical constants of zinc oxide thin films by ellipsometry with various models, *Thin Solid Films*, 2006, **510**, 32–38.
7 R. Kerremans, C. Kaiser, W. Li, N. Zarrabi, P. Meredith and A. Armin, The Optical Constants of Solution-Processed Semiconductors—New Challenges with Perovskites and Non-Fullerene Acceptors*Adv*, *Opt. Mater.*, 2020, **8**, 2000319.
8 M. S. Alias, I. Dursun, M. I. Saidaminov, E. M. Diallo, P. Mishra, T. K. Ng, O. M. Bakr and B. S. Ooi, Optical constants of $CH_3NH_3PbBr_3$ perovskite thin films measured by spectroscopic ellipsometry, *Opt. Express*, 2016, **24**, 16586–16594.
9 Y. Jiang, M. A. Green, R. Sheng and A. Ho-Baillie, Room temperature optical properties of organic–inorganic lead halide perovskites, *Sol. Energy Mater. Sol. Cells*, 2015, **137**, 253–257.
10 P. Loeper, M. Stuckelberger, B. Niesen, J. Werner, M. Filipic, S. J. Moon, J. H. Yum, M. Topic, S. De Wolf and C. Ballif, Complex Refractive Index Spectra of $CH_3NH_3PbI_3$ Perovskite Thin Films Determined by Spectroscopic Ellipsometry and Spectrophotometry, *J. Phys. Chem. Lett.*, 2015, **6**, 66–71.
11 A. M. A. Leguy, P. Azarhoosh, M. I. Alonso, M. Campoy-Quiles, O. J. Weber, J. Yao, D. Bryant, M. T. Weller, J. Nelson, A. Walsh, M. Van Schilfgaarde and P. R. F. Barnes, Experimental and theoretical optical properties of methylammonium lead halide perovskites, *Nanoscale*, 2016, **8**, 6317–6327.
12 C. He, G. Zha, C. Deng, Y. An, R. Mao, Y. Liu, Y. Lu and Z. Chen, Refractive Index Dispersion of Organic–Inorganic

 

Hybrid Halide Perovskite $CH_3NH_3PbX_3$ (X=Cl, Br, I) Single Crystals, *Cryst. Res. Technol.*, 2019, **54**, 1900011.

13 M. I. Alonso, B. Charles, A. Francisco-López, M. Garriga, M. T. Weller and A. R. Goñi, Spectroscopic ellipsometry study of $FA_xMA_{1-x}PbI_3$ hybrid perovskite single crystals, *J. Vac. Sci. Technol., B: Nanotechnol. Microelectron.: Mater., Process., Meas., Phenom.*, 2019, **37**, 062901.

14 M. Zhao, Y. Shi, J. Dai and J. Lian, Ellipsometric study of the complex optical constants of a $CsPbBr_3$ perovskite thin film, *J. Mater. Chem. C*, 2018, **6**, 10450–10455.

15 M. Anaya, G. Lozano, M. E. Calvo, W. Zhang, M. B. Johnston, H. J. Snaith and H. Míguez, Optical description of mesostructured organic–inorganic halide perovskite solar cells, *J. Phys. Chem. Lett.*, 2015, **6**, 48–53.

16 J. Ávila, C. Momblona, P. Boix, M. Sessolo, M. Anaya, G. Lozano, K. Vandewal, H. Míguez and H. J. Bolink, High voltage vacuum-deposited $CH_3NH_3PbI_3$–$CH_3NH_3PbI_3$ tandem solar cells, *Energy Environ. Sci.*, 2018, **11**, 3292–3297.

17 Q. Lin, A. Armin, R. C. R. Nagiri, P. L. Burn and P. Meredith, Electro-optics of perovskite solar cells, *Nat. Photonics*, 2014, **9**, 106–112.

18 M. E. Calvo, Materials chemistry approaches to the control of the optical features of perovskite solar cells, *J. Mater. Chem. A*, 2017, **5**, 20561–20578.

19 G. Li, F. W. R. Rivarola, N. J. L. K. Davis, S. Bai, T. C. Jellicoe, F. de la Peña, S. Hou, C. Ducati, F. Gao, R. H. Friend, N. C. Greenham and Z. K. Tan, Highly efficient perovskite nanocrystal light-emitting diodes enabled by a universal crosslinking method, *Adv. Mater.*, 2016, **28**, 3528–3534.

20 G. Lozano, The Role of Metal Halide Perovskites in Next-Generation Lighting Devices, *J. Phys. Chem. Lett.*, 2018, **9**, 3987–3997.

21 J. Jean, Getting high with quantum dot solar cells, *Nat. Energy*, 2020, **5**, 10–11.

22 M. Hao, Y. Bai, S. Zeiske, L. Ren, J. Liu, Y. Yuan, N. Zarrabi, N. Cheng, M. Ghasemi, P. Chen, M. Lyu, D. He, J.-H. Yun, Y. Du, Y. Wang, S. Ding, A. Armin, P. Meredith, G. Liu, H.-M. Cheng and L. Wang, Ligand-Assisted Cation-Exchange Engineering for High-Efficiency Colloidal $Cs_{1-x}FA_xPbI_3$ Quantum Dot Solar Cells with Reduced Phase Segregation, *Nat. Energy*, 2020, **5**, 79–88.

23 S. Zhou, G. Zhou, Y. Li, X. Xu, Y.-J. Hsu, J. Xu, N. Zhao and X. Lu, Understanding Charge Transport in All-Inorganic Halide Perovskite Nanocrystal Thin-Film Field Effect Transistors, *ACS Energy Lett.*, 2020, **5**, 2614–2623.

24 P. Ramasamy, D. H. Lim, B. Kim, S. H. Lee, M. S. Lee and J. S. Lee, All-inorganic cesium lead halide perovskite nanocrystals for photodetector applications, *Chem. Commun.*, 2016, **52**, 2067–2070.

25 Q. Chen, J. Wu, X. Ou, B. Huang, J. Almutlaq, A. A. Zhumekenov, X. Guan, S. Han, L. Liang, Z. Yi, J. Li, X. Xie, Y. Wang, Y. Li, D. Fan, D. B. L. Teh, A. H. All, O. F. Mohammed, O. M. Bakr, T. Wu, M. Bettinelli, H. Yang, W. Huang and X. Liu, All-Inorganic Perovskite Nanocrystal Scintillators, *Nature*, 2018, **561**, 88–93.

26 A. Rubino, T. Huq, J. Dranczewski, G. Lozano, M. E. Calvo, S. Vezzoli, H. Míguez and R. Sapienza, *J. Mater. Chem. C*, 2020, **8**, 15990–15995.

27 M. Athanasiou, P. Papagiorgis, A. Manoli, C. Bernasconi, M. I. Bodnarchuk, M. V. Kovalenko and G. Itskos, *ACS Photonics*, 2021, **8**, 2120–2129.

28 J.-P. Correa-Baena, M. Anaya, G. Lozano, W. Tress, K. Domanski, M. Saliba, T. Matsui, T. J. Jacobsson, M. E. Calvo, A. Abate, M. Grätzel, H. Míguez and A. Hagfeldt, Unbroken perovskite: interplay of morphology, electro-optical properties and ionic movement, *Adv. Mater.*, 2016, **28**, 5031–5037.

29 L. Protesescu, S. Yakunin, M. I. Bodnarchuk, F. Krieg, R. Caputo, C. H. Hendon, R. X. Yang, A. Walsh and M. V. Kovalenko, Nanocrystals of Cesium Lead Halide Perovskites ($CsPbX_3$, X=Cl, Br, and I): Novel Optoelectronic Materials Showing Bright Emission with Wide Color Gamut, *Nano Lett.*, 2015, **15**, 3692–3696.

30 J. Shamsi, A. S. Urban, M. Imran, L. De Trizio and L. Manna, *Chem. Rev.*, 2019, **119**, 3296–3348.

31 D. B. Dement, M. Puri and V. E. Ferry, Determining the Complex Refractive Index of Neat CdSe/CdS Quantum Dot Films, *J. Phys. Chem. C*, 2018, **122**, 21557–21568.

32 P. Geiregat, Y. Justo, S. Abe, S. Flamee and Z. Hens, Giant and broad-band absorption enhancement in colloidal quantum dot monolayers through dipolar coupling, *ACS Nano*, 2013, **7**, 987–993.

33 D. D. W. Grinolds, P. R. Brown, D. K. Harris, V. Bulovic and M. G. Bawendi, Quantum-dot size and thin-film dielectric constant: precision measurement and disparity with simple models, *Nano Lett.*, 2015, **15**, 21–26.

34 E. S. Skibinsky-Gitlin, S. Rodríguez-Bolívar, M. Califano and F. M. Gómez-Campos, Optical properties of nanocrystal films: blue shifted transitions as signature of strong coupling, *Nanoscale Adv.*, 2020, **2**, 384–393.

35 A. Rubino, L. Caliò, M. E. Calvo and H. Míguez, Ligand-Free $MAPbI_3$ Quantum Dot Solar Cells Based on Nanostructured Insulating Matrices, *Sol. RRL*, 2021, 2100204.

36 M. Anaya, A. Rubino, T. C. Rojas, J. F. Galisteo-López, M. E. Calvo and H. Míguez, Strong quantum confinement and fast photoemission activation in $CH_3NH_3PbI_3$ perovskite nanocrystals grown within periodically mesostructured films, *Adv. Opt. Mater.*, 2017, **5**, 1601087.

37 A. Rubino, M. Anaya, J. F. Galisteo-López, T. C. Rojas, M. E. Calvo and H. Míguez, Highly Efficient and Environmentally Stable Flexible Color Converters Based on Confined $CH_3NH_3PbBr_3$ Nanocrystals, *ACS Appl. Mater. Interfaces*, 2018, **10**, 38334–38340.

38 D. Poelman and P. F. Smet, Methods for the determination of the optical constants of thin films from single transmission measurements: a critical review, *J. Phys. D: Appl. Phys.*, 2003, **1850**, 1850–1857.

39 S. Brittman and E. C. Garnett, Measuring n and k at the Microscale in Single Crystals of $CH_3NH_3PbBr_3$ Perovskite, *J. Phys. Chem. C*, 2016, **120**, 616–620.

40 G. A. Niklasson, C. G. Granqvist and O. Hunderi, Effective medium models for the optical properties of inhomogeneous materials, *Appl. Opt.*, 1981, **20**, 26–30.
41 J. Xie, Y. Liu, J. Liu, L. Lei, Q. Gao, J. Li and S. Yang, Study on the correlations between the structure and photoelectric properties of $CH_3NH_3PbI_3$ perovskite light-harvesting material, *J. Power Sources*, 2015, **285**, 349–353.
42 L. E. Brus, Electron–electron and electron–hole interactions in small semiconductor crystallites: The size dependence of the lowest excited electronic state, *J. Chem. Phys.*, 1984, **80**, 4403.
43 J. Tauc, R. Grigorovic and A. Vancu, Optical Properties and Electronic Structure of Amorphous Germanium, *Phys. Status Solidi B*, 1966, **15**, 627–637.
44 B. D. Viezbicke, S. Patel, B. E. Davis and D. P. Birnie III, Evaluation, of the Tauc method for optical absorption edge determination: ZnO thin films as a model system, *Phys. Status Solidi B*, 2015, **252**, 1700–1710.
45 O. Levy and E. Cherkaev, Effective medium approximations for anisotropic composites with arbitrary component orientation, *J. Appl. Phys.*, 2013, **114**, 164102.
46 N. Hidalgo, C. López-López, G. Lozano, M. E. Calvo and H. Míguez, Characterization of Mesoporous Thin Films by Specular Reflectance Porosimetry, *Langmuir*, 2012, **28**, 13777–13782.
47 A. R. Forouhi and I. Bloomer, Optical dispersion relations for amorphous semiconductors and amorphous dielectrics, *Phys. Rev. B: Condens. Matter Mater. Phys.*, 1986, **34**, 7018.
48 T. Vossmeyer, L. Katsikas, M. Giersig, I. G. Popovic, K. Diesner, A. Chemseddine, A. Eychmueller and H. Weller, CdS Nanoclusters: Synthesis, Characterization, Size Dependent Oscillator Strength, Temperature Shift of the Excitonic Transition Energy, and Reversible Absorbance Shift, *J. Phys. Chem.*, 1994, **98**, 7665–7673.
49 Y. Kayanuma, Quantum-size effects of interacting electrons and holes in semiconductor microcrystals with spherical shape, *Phys. Rev. B: Condens. Matter Mater. Phys.*, 1988, **38**, 9797.
50 N. J. Turro, *Molecular Photochemistry*, W. A. Benjamin, Inc., Reading, MA, 1965.
51 M. Baranowski and P. Plochocka, Excitons in Metal-Halide Perovskites, *Adv. Energy Mater.*, 2020, **10**, 1903659.
52 I. Angeloni, R. Raja, A. Brescia, F. Polovitsyn, M. De Donato, G. Canepa, R. Bertoni, P. Zaccaria and I. Moreels, Disentangling the Role of Shape, Ligands, and Dielectric Constants in the Absorption Properties of Colloidal CdSe/CdS Nanocrystals, *ACS Photonics*, 2016, **3**, 58–67.
53 S. J. Lim, M. U. Zahid, P. Le, L. Ma, D. Entenberg, A. S. Harney, J. Condeelis and A. M. Smith, Brightness-equalized quantum dots, *Nat. Commun.*, 2015, **6**, 1–10.
54 T. Takagahara, Effects of dielectric confinement and electron-hole exchange interaction on excitonic states in semiconductor quantum dots, *Phys. Rev. B: Condens. Matter Mater. Phys.*, 1993, **47**, 4569.
55 C. Giansante, I. Infante, E. Fabiano, R. Grisorio, G. P. Suranna and G. Gigli, Darker-than-Black" PbS Quantum Dots: Enhancing Optical Absorption of Colloidal Semiconductor Nanocrystals via Short Conjugated Ligands, *J. Am. Chem. Soc.*, 2015, **137**, 1875–1886.
56 I. Moreels, D. Kruschke, P. Glas and J. W. Tomm, The dielectric function of PbS quantum dots in a glass matrix, *Opt. Mater. Express*, 2012, **2**, 496–500.
57 S. Masi, C. Echeverría-Arrondo, K. M. M. Salim, T. T. Ngo, P. F. Mendez, E. López-Fraguas, D. F. Macias-Pinilla, J. Planelles, J. I. Climente and I. Mora-Seró, Chemi-Structural Stabilization of Formamidinium Lead Iodide Perovskite by Using Embedded Quantum Dots, *ACS Energy Lett.*, 2020, **5**, 418–427.
58 J. Xu, W. Huang, P. Li, D. R. Onken, C. Dun, Y. Guo, K. B. Ucer, C. Lu, H. Wang and S. M. Geyer, Imbedded nanocrystals of $CsPbBr_3$ in Cs4PbBr6: kinetics, enhanced oscillator strength, and application in light-emitting diodes, *Adv. Mater.*, 2017, **29**, 1703703.

 